ACS APPLIED MATERIALS & INTERFACES

Research Article

Cite This: ACS Appl. Mater. Interfaces XXXX, XXX, XXX−XXX

www.acsami.org

Self-Strengthened Oxidation-Responsive Bioactivating Prodrug Nanosystem with Sequential and Synergistically Facilitated Drug Release for Treatment of Breast Cancer

Kaiyuan Wang,[†,¶] Bin Yang,[†,¶] Hao Ye,[†] Xuanbo Zhang,[†] Hang Song,[†] Xia Wang,[‡] Na Li,[§] Lin Wei,[∥] Yu Wang,[†] Haotian Zhang,[⊥] Qiming Kan,[⊥] Zhonggui He,[†] Dun Wang,[*,#] and Jin Sun[*,†]

[†]Department of Pharmaceutics, Wuya College of Innovation, [‡]School of Pharmacy, [§]Clinical Pharmacy, Wuya College of Innovation, [⊥]School of Life Science and Biopharmaceutics, and [#]Key Laboratory of Structure-Based Drug Design & Discovery of Ministry of Education, Shenyang Pharmaceutical University, Shenyang, Liaoning 110016, P. R. China

[∥]Key Laboratory of Microbiology, School of Life Science, Heilongjiang University, Harbin 150080, P. R. China

Supporting Information

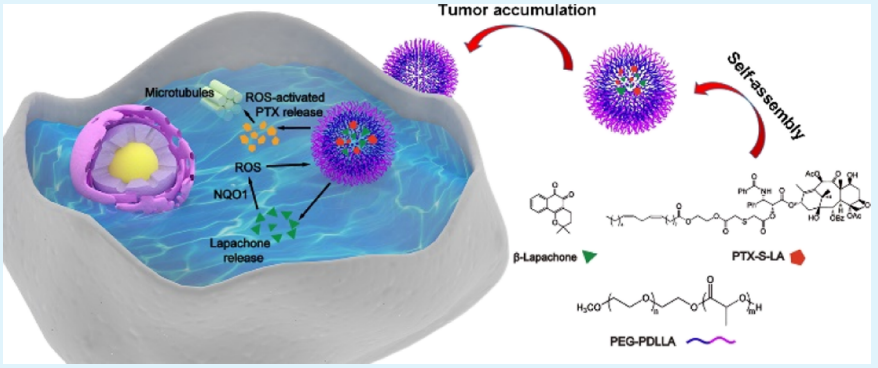

ABSTRACT: Although environment-sensitive prodrug-based nanoparticles (NPs) have developed rapidly, lots of prodrug NPs still show poor selectivity and efficiency of parent drug bioactivation because of tumor heterogeneity. Herein, self-strengthened bioactivating prodrug-based NPs are fabricated via co-encapsulation of oxidation-responsive thioether-linked linoleic acid-paclitaxel conjugates (PTX-S-LA) and *β*-lapachone (LPC) into polymeric micelles (PMs). Following cellular uptake, PMs first release LPC to significantly elevate the reactive oxidative species (ROS) level through NAD(P)H: quinone oxidoreductase-1 (NQO1) catalysis. Then, NQO1-generated ROS in combination with endogenous high ROS levels in tumor cells could synergistically facilitate PTX-S-LA to release the active cytotoxic agent PTX. Such a novel prodrug nanosystem exhibits self-strengthened prodrug bioactivation, ultraselective release, and cytotoxicity between cancer and normal cells, prolonged circulation time, and enhanced tumor accumulation, leading to high antitumor efficiency and superior biosafety. Our findings pave the new way for the rational design of oxidation-responsive prodrug NPs for high-efficacy cancer chemotherapy.

KEYWORDS: *paclitaxel, β-lapachone, self-strengthened nanoparticles, oxidation-responsive prodrug, sequential drug release*

1. INTRODUCTION

Malignant tumors remain the leading disease threatening human health. In spite of representing a backbone in clinical cancer therapy, chemotherapy is still far from satisfactory due to the limited antitumor efficacy and serious side effects resulting from poor tumor selectivity.[1] It is well known that anaerobic glycolysis, leaky vasculature, tissue hypoxia, lower pH are typical characteristics of tumor microenvironment. Thus, stimuli-responsive prodrugs responding to different tumor-specific biotriggers have been developed rapidly to overcome the above limitations over the past few decades.[2−5]

Tumor cells generally exhibit high oxidative/reduction stress, and the reactive oxygen species (ROS) concentration of tumor is usually 10−50 times higher than that of normal cells. Therefore, oxidation-responsive prodrugs could realize tumor-specific bioactivation.[6,7] Oxidation-responsive prodrug strategies containing different covalent bond linkages, such as thioketal,[8] boronic ester,[9,10] and selenium[11] have been widely applied for chemotherapy. However, in terms of the tumor ROS heterogeneity, the specificity and efficacy of oxidation-responsive drug release is still far from satisfactory to achieve desirable antitumor efficiency and low toxicity. Herein, we hypothesize the unique self-strengthened oxidation-responsive prodrug-based nanosystem, combining exogenous-generated ROS with endogenous high ROS levels in tumor cells,

Received: February 18, 2019
Accepted: May 6, 2019
Published: May 6, 2019

DOI: 10.1021/acsami.9b03056
ACS Appl. Mater. Interfaces XXXX, XXX, XXX−XXX

Scheme 1. Schematic Representation of an Oxidation-Responsive Prodrug-Based Nanosystem with Sequential and Synergistically Facilitated Drug Release[a]

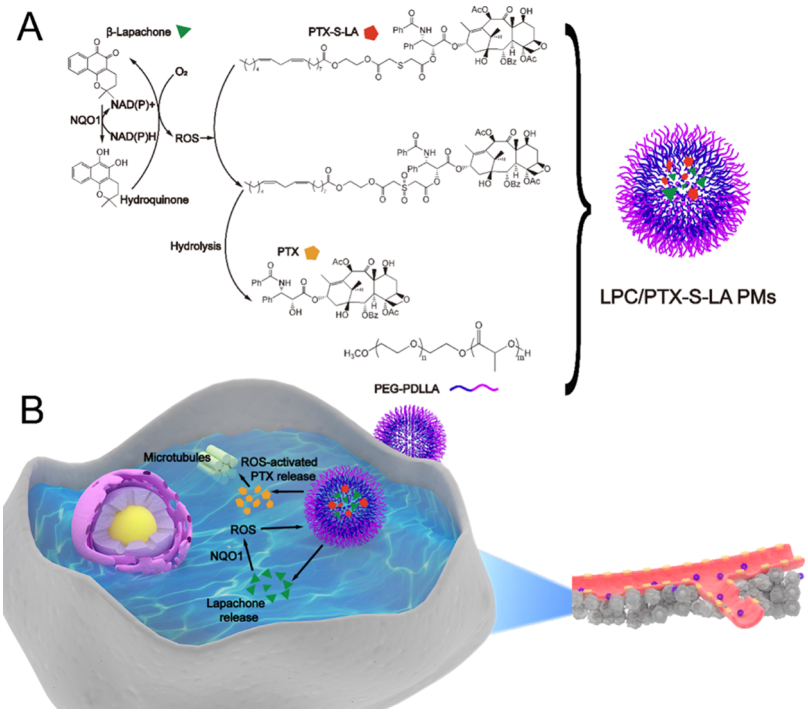

[a](A) Structure of PTX-S-LA, *β*-Lapachone and PEG−PDLLA. (B) Prodrug-based nanosystem would accumulate in cancer owing to the EPR effect; following cellular uptake, nanosystem release LPC first, remarkably raising the oxidative stress level via the catalysis of tumor-overexpressing NQO1, inducing a sequential and synergistically facilitated release of PTX from PTX-S-LA.

facilitating prodrug bioactivation to overcome ROS heterogeneity in tumors.

Lapachone (LPC) is extracted from plants and is a typical substrate of NQO1.[12] NQO1 could protect cells from quinones by catalyzing two-electron reduction.[13] LPC is activated by NQO1 to generate a considerable number of ROS via the NQO1-mediated redox cycle to elicit the anticancer effect. Because the NQO1 level is overexpressed in various tumor cells, LPC shows a specific antitumor activity and could facilitate ROS-triggered release of oxidation-responsive prodrugs in tumor cells.

To test our hypothesis, we prepared an oxidation-responsive self-strengthened prodrug-based polymeric micelles (LPC/PTX-S-LA PMs) through co-encapsulation of an oxidation-responsive paclitaxel (PTX) prodrug (PTX-S-LA) and LPC into poly(ethylene glycol)-*b*-poly(D,L-lactic acid) (PEG−PDLLA) PMs.[14−16] The LPC/PTX-S-LA PMs would release LPC first after cellular uptake and then selectively increase the intracellular ROS level of cancer through the NQO1-mediated redox cycle. LPC-induced ROS together with endogenous ROS overproduced in tumor cells synergistically facilitates bioactive PTX release from prodrug PTX-S-LA, exhibiting ultraselective bioactivation and cytotoxicity between cancer and normal cells (Scheme 1). Integrating NQO1-induced ROS production and ROS-triggered PTX chemotherapy into PMs demonstrate a paradigm of oxidation-responsive prodrug-based nanoparticles (NPs) for high-efficacy cancer therapy.[17]

2. EXPERIMENTAL SECTION

2.1. Materials. The PEG5k−PDLLA5k block copolymer was bought from DaiGang Biotechnology Co., Ltd., China. *β*-Lapachone was obtained from Nanjing Sheng Sai Chemical Co., Ltd., China. Paclitaxel was bought from NanJing Jingzhu biotechnology Co., Ltd., China. Glycol, linoleic acid, thiodiglycolic anhydride, 4-dimethylaminopyridine (DMAP), *N*-(3-dimethylaminopropyl)-*N*′-ethylcarbodiimide hydrochloride (EDCI), 1-hydroxybenzotriazole monohydrate (HOBt) were obtained from Energy Chemical Co., Ltd., China. Hoechst and Coumarin-6 (C-6) were bought from Sigma-Aldrich, USA. DiR and DCFH-DA were obtained from Dalian Meilun Biotechnology Co., Ltd., China. The NQO1 ELISA kit was purchased from Shanghai Jianglai industrial Limited By Share Ltd., China.

2.2. Synthesis of PTX-S-LA. Ethylene glycol (76 mL), *P*-toluenesulfonic acid (0.85 g), and linoleic acid (4.2 g) were stirred in the flask for 3 h at 110 °C under nitrogen. After extracting using methylbenzene, washing with $NaHCO_3$ solution, and dried under vacuum; the linoleic acid ethyl ester was purified through column chromatography. The yield was 62.3%. Then, 0.5 g HOBt, 0.64 g EDCI, and 0.44 g thiodiglycolic anhydride were dissolved into 20 mL dichloromethane. The linoleic acid ethyl ester was dropped to a mixture in an ice bath for 40 min reaction. Then, the temperature was raised to 25 °C and continued to react for another 12 h. After evaporating dichloromethane, hydrochloric acid and extracted product with dichloromethane were added; then, the dichloromethane layer was washed using NaCl solution and dried with sodium sulfate. 2′-*O*-(2-oxo-2-(2-((*Z*)-linoleoyloxy)ethoxy)ethylsulfenyl) acetic acid was purified using column chromatography. The yield was 53.8%. Then, 1 g EDCI, 4.4 g PTX, 2.8 g 2′-*O*-(2-oxo-2-(2-((*Z*)-linoleoyloxy)ethoxy)ethylsulfenyl) acetic acid, and 0.7 g HOBt into dichloromethane were dissolved, stirred for 2 h in an ice bath and reacted for 48 h at 25 °C. After evaporating to remove dichloromethane, pure PTX-S-LA was obtained using preparative liquid chromatography. The yield was 47.3%.

2.3. Synthesis of PTX-LA. PTX (99 mg, 116 mmol), DMAP (14 mg, 116 mmol), and DCC (48 mg, 234 mmol) were dissolved into 15 mL dichloromethane. Linoleic acid (32 mg, 116 mmol) was added and stirred at 25 °C for 24 h. After evaporating to remove

DOI: 10.1021/acsami.9b03056
ACS Appl. Mater. Interfaces XXXX, XXX, XXX−XXX

dichloromethane, pure PTX-LA was obtained using preparative liquid chromatography. The yield was 48.5%.

2.4. Fabrication and Characterization of the Nanosystem. PTX-S-LA (3 mg, 2.3 mmol) or PTX-LA (2.56 mg, 2.3 mmol), β-lapachone (2.13 mg, 8.8 mmol), and PEG−PDLLA (30 mg) into 7 mL acetonitrile were dissolved. The thin film was formed by rotary evaporation at 60 °C. Normal saline (4 mL) was added and sonicated for 5 min. Resulted solution was filtered with a 220 nm aperture filter to remove large particles. Then, encapsulation percentage and loading density were monitored using HPLC. To measure the concentration of PTX prodrugs and LPC, the absorption wavelengths were set at 227 and 260 nm. The morphology and particle size of prepared PMs were measured through a transmission electron microscope (Hitachi HT7700) and dynamic light scattering (Malvern, U.K.), respectively. The colloidal stability of LPC/prodrug PMs was tested subsequently in phosphate-buffered saline (PBS) containing 10% fetal bovine serum (FBS) and PBS containing 30% ethanol at 37 °C for 24 h. The diameter was monitored using dynamic light scattering at preset time points.

2.5. ROS Responsiveness Test of PTX Prodrugs. The PTX prodrug (PTX-S-LA or PTX-LA) in PBS containing 30% ethanol solutions with H_2O_2 concentrations of 0, 3, 5, and 10 mM[3,4,6,7,11,18] was incubated at 37 °C. At predetermined time points, a solution of 500 μL was withdrawn for analysis using HPLC.

2.6. Drug Release Performances. Prepared LPC/prodrug PMs were dissolved in PBS and divided into different groups, including 0, 3, 5, and 10 mM H_2O_2 groups. The solution of each group was added in a dialysis bag, and dialysis was performed with 30 mL PBS containing 30% ethanol. At predetermined time points, a sample of 500 μL was taken to analyze using HPLC.

2.7. Cell Culture. 4T1, A549, and NIH 3T3 cells bought from ATCC were cultured in RPMI 1640, high-glucose Dulbecco's modified Eagle's medium and DME/F12 medium, respectively, supplemented with 1% penicillin/streptomycin and 10% FBS under the humidified atmosphere at 37 °C.

2.8. Cell Uptake and Intracellular PTX Release. 4T1 cells (100 000 cells/well) were seeded into 12-well plates and cultivated for 24 h, and then cells were exposed to C-6-Sol and C-6-PDLLA−PEG for 0.5 and 2 h, respectively. After washing with cold PBS thrice and 4% paraformaldehyde, cells were washed and the nuclei were counterstained using Hoechst. Then, the cover slips were observed using a confocal laser scanning microscope (CLSM). Mean fluorescence intensity was quantified using ImageJ.

For flow cytometry examination, 4T1 cells (100 000 cells/well) were seeded into 12-well plates and incubated for 24 h, and then cells were exposed to C-6-Sol and C-6-PDLL−PEG for 0.5 and 2 h, respectively. Finally, the cells were collected in tubes and suspended with PBS. The intracellular fluorescence signal was examined with a FACS calibur flow cytometer and analyzed with FlowJo software.

To measure the released PTX from PMs (PTX equivalent of 500 ng/mL) when incubating 4T1, A549, and NIH 3T3 cells with free PTX and prodrug micelles for 6 or 24 h, cells as well as culture media were gathered, sonicated, and centrifuged to acquire the sample. Then, 50 μL sample, 50 μL diazepam (internal standard), and 250 μL acetonitrile were mixed, vortexed, and centrifuged to obtain the supernatant. Concentration of PTX in the supernatant was monitored using UPLC-MS-MS (Waters Co., Ltd.). Free PTX was set as a control group, and the PTX release ratio was calculated as follows: PTX released from prodrug micelles/PTX measured in control group ×100%.

2.9. Cytotoxicity Assays. The cytotoxicity of PTX, LPC, PTX prodrug micelles, and LPC/prodrug PMs against 4T1, A549, and NIH 3T3 cells was evaluated using MTT assay. Briefly, cells (1500 cells/well) were seeded into 96-well plates. After preincubation for 12 h, cells were exposed to serial dilutions of the drugs and incubated for 48 h. Untreated cells were used as the control. At the end of the incubation, medium was replaced with MTT. After 4 h cultivation, the MTT medium solution was removed carefully, 0.1 mL dimethyl sulfoxide was added to the wells and the plate was shaken to dissolve the precipitate. Finally, the absorbency of the sample was measured on a microplate reader at 570 nm.

2.10. Intracellular ROS Production and NQO1 Level Quantification. To observe ROS-induced fluorescence, 4T1 cancer cells and NIH 3T3 cells (50 000 cells/well) were seeded into 24-well plates and cultivated for 24 h, and then cells were exposed to 0.8 μM PTX-S-LA PMs, 0.8 μM PTX-LA PMs, LPC/PTX-LA PMs (2.4 μM LPC, 0.8 μM PTX-LA), or LPC/PTX-S-LA PMs (2.4 μM LPC, 0.8 μM PTX-S-LA) for 3 h. Then, the cells were stained with DCFH-DA for half an hour, washed thrice using PBS. Finally, the intracellular fluorescence signal was monitored using an inverted fluorescence microscope. Mean fluorescence intensity was quantified using ImageJ.

For quantitative examination, 4T1 cells and NIH 3T3 cells (100 000 cells/well) were seeded into 12-well plates and cultivated for 24 h, and then cells were exposed to 0.5 μM PTX-S-LA PMs, 0.5 μM PTX-LA PMs, LPC/PTX-LA PMs (1.5 μM LPC, 0.5 μM PTX-LA), or LPC/PTX-S-LA PMs (1.5 μM LPC, 0.5 μM PTX-S-LA) for 1, 3, 6, and 12 h. Then, the cells were stained with DCFH-DA for half an hour and washed thrice using PBS. At last, cells were collected in tubes and suspended with PBS. The intracellular fluorescence signal was examined with the FACSCalibur flow cytometer and analyzed with FlowJo software.

To reveal differences in NQO1 levels between 4T1, A549, and NIH 3T3 cells, NQO1 quantification was performed according to purchased ELISA kit instructions (Shanghai Jianglai industrial Limited By Share Ltd.). The optical density of the sample was measured on a microplate reader at 450 nm.

2.11. Animal Studies. Animal studies were conducted according to the Guide for Care and Use of Laboratory Animals of Shenyang Pharmaceutical University.

2.12. Pharmacokinetics. Sprague Dawley rats (210−260 g, n = 3) were injected intravenously with Taxol, LPC/PTX-S-LA PMs, and LPC/PTX-LA PMs (4 mg kg^{-1} of PTX). At timed intervals, 400 μL of blood was collected and centrifuged to acquire plasma. Then 50 μL of plasma, 50 μL of diazepam (internal standard), and 250 μL of acetonitrile were mixed, vortexed, and centrifuged to obtain the supernatant. Concentration of PTX, PTX-S-LA, and PTX-LA in the supernatant was monitored with UPLC-MS-MS (Waters Co., Ltd.).

2.13. Biodistribution and PTX Release and LPC Accumulation in the Tumor. 4T1 tumor-bearing mice were utilized for the biodistribution experiment.[19] Free DiR and DiR-labeled PEG−PDLLA micelles (2 mg kg^{-1} for DiR) were injected intravenously until tumor volume was 300 mm^3. Optical imaging was conducted at 4, 8, 12, and 24 h after injection at an excitation of 748 nm. Then, the mice were killed at 24 h, and fluorescence in organs and tumors was analyzed with a small-animal imaging system.

The tumor bioactivation of prodrug micelles were examined by 4T1 tumor-bearing mice. Once tumor grew to 300 mm^3, the prodrug micelles (8 mg kg^{-1} for PTX, 6.8 mg kg^{-1} for LPC) were administrated intravenously. The mice were killed at 12 h post injection; tumors were excised, weighed, and homogenized to obtain the homogenate. Then, 50 μL of homogenate, 50 μL of diazepam (internal standard), and 250 μL of acetonitrile were mixed, vortexed, and centrifuged to obtain the supernatant. Concentrations of PTX and LPC in the supernatant were monitored with UPLC-MS-MS (Waters Co., Ltd.).

2.14. In Vivo Anticancer Activity. To establish the xenograft tumor model, 4T1 cancer cells were inoculated to BALB/c mice. Once tumor size was around 100 mm^3, mice were randomized to seven groups, and saline, PTX-LA PMs, LPC PMs, Taxol, LPC/PTX-LA PMs, PTX-S-LA PMs, or LPC/PTX-S-LA PMs were administrated intravenously to mice every other day (8 mg kg^{-1} for PTX, 6.8 mg kg^{-1} for LPC). Ten days after first administration, mice were killed humanely and excised and the major organ as well as tumor was fixed by 4% paraformaldehyde for hematoxylin and eosin.

2.15. Statistical Analysis. Data were displayed as mean ± SD. Comparison of groups was judged using one-way ANOVA and student's t-test; difference was considered significant when $P < 0.05$.

DOI: 10.1021/acsami.9b03056
ACS Appl. Mater. Interfaces XXXX, XXX, XXX−XXX

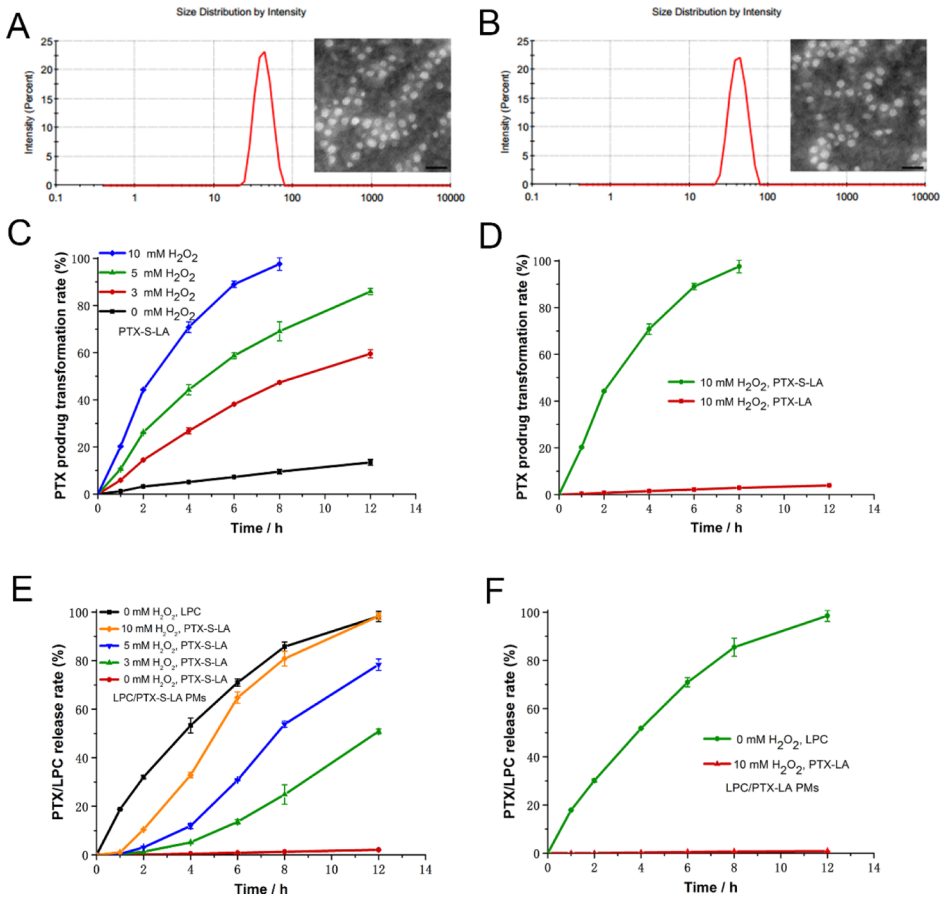

Figure 1. Size and morphology of LPC/PTX-S-LA PMs (A) and LPC/PTX-LA PMs (B); the scale bar represents 100 nm. Transformation of PTX-S-LA (C) and PTX-LA (D) to PTX when incubated with H_2O_2. Drug release kinetics of LPC and PTX from LPC/PTX-S-LA PMs (E) and LPC/PTX-LA PMs (F) in PBS complemented with 30% ethanol under H_2O_2.

3. RESULTS AND DISCUSSIONS

3.1. Synthesis of PTX-S-LA and PTX-LA. The ROS-activated PTX prodrug (PTX-S-LA) was synthesized by coupling linoleic acid to PTX through thioether linkage. Additionally, PTX-LA was synthesized as a nonsensitive control. As shown in Figures S1 and S2, structures of PTX-S-LA and PTX-LA were verified using MS and ^{1}H NMR.

3.2. Fabrication and Characterization of the Nanosystem. LPC/PTX-S-LA PMs were fabricated through the thin-film hydration method.[20] The drug loading efficiencies of PTX-S-LA, PTX-LA, and LPC in the PEG−PDLLA micelles were 16.41, 16.47, and 4.39%, and the relevant encapsulation percentages were 98.44, 98.86, and 48.34%, respectively. Compared with LPC micelles, the LPC/PTX-S-LA PMs exhibited much higher loading density as well as encapsulation percentage of LPC, probably owing to inhibition of LPC crystallization by co-encapsulated PTX-S-LA.[21] As shown in Figure 1A,B, the average diameter of LPC/PTX-S-LA PMs was around 40 nm with regularly spherical-shaped structures. LPC/PTX-S-LA PMs could remain stable without notable change in particle size for 24 h in PBS complemented with 10% FBS and PBS complemented with 30% ethanol at 37 °C (Figure S3), demonstrating their good colloidal stabilities under simulated physiological conditions.

3.3. ROS Responsiveness Test of PTX Prodrugs. The PTX-S-LA prodrug was investigated for ROS-responsive bioactivation, with H_2O_2 being a usual ROS simulant. As shown in Figure 1, PTX-S-LA released only about 13% of PTX in the absence of H_2O_2 for 12 h. By contrast, almost 100% PTX was released when incubated with 10 mM H_2O_2 in 8 h. As for the nonsensitive control, PTX-LA released no more than 4% PTX when incubated with 10 mM H_2O_2 for 12 h. The results suggested that PTX-S-LA had excellent oxidation sensitivity to ROS.

3.4. Drug Release Performances. To explore the role of ROS in accelerating the active PTX release, LPC/PTX-S-LA PMs containing 30% ethanol was sealed in dialysis bags under various H_2O_2 concentrations. After 4 h incubation, micelles released about 50% LPC and less than 1% PTX-S-LA without H_2O_2 because very hydrophobic prodrug PTX-S-LA is very difficult to be hydrolyzed. Under oxidative stress conditions, the thioether bond was oxidized into the relatively hydrophilic sulfoxide or sulphone groups, thus allowing for rapid prodrug hydrolysis to release PTX.[18] As shown in Figure 1E,F, the H_2O_2-triggered PTX release from PTX-S-LA PMs was in a concentration-dependent manner, reaching 98% within 8 h when incubated with 10 mM H_2O_2. By contrast, PTX-LA PMs did not exhibit any release of PTX even in 10 mM H_2O_2 for 12 h because of the high hydrophobicity and poor bioactivation performance of PTX-LA.

3.5. Cell Uptake and Intracellular PTX Release. C-6 and C-6-labeled PEG−PDLLA micelles were utilized to examine cell uptake of prodrug-based PMs.[22] The 4T1 cell uptake of C-6 or C-6-labeled PMs were time-dependent, and the C-6-labeled PMs showed remarkably stronger fluorescence than C-6 solution for both 0.5 and 2 h (Figures 2A−C and S4).

DOI: 10.1021/acsami.9b03056
ACS Appl. Mater. Interfaces XXXX, XXX, XXX−XXX

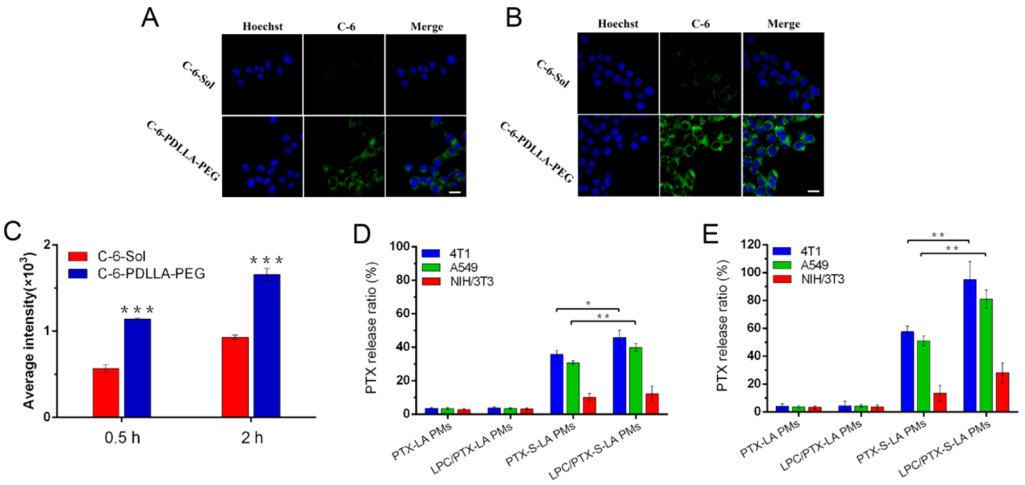

Figure 2. CLSM images of 4T1 cancer cells after incubation with C-6-Sol and C-6-PDLLA−PEG at 0.5 h (A) and 2 h (B). Scale bar, 15 μm. (C) Quantification using flow cytometry for cell uptake in 4T1 cancer cells. Differences from C-6-Sol, ***$P < 0.001$. PTX release from PMs when incubated in 4T1, A549, and NIH 3T3 cells for 6 h (D) and 24 h (E). (**$P < 0.01$, *$P < 0.05$, $n = 3$).

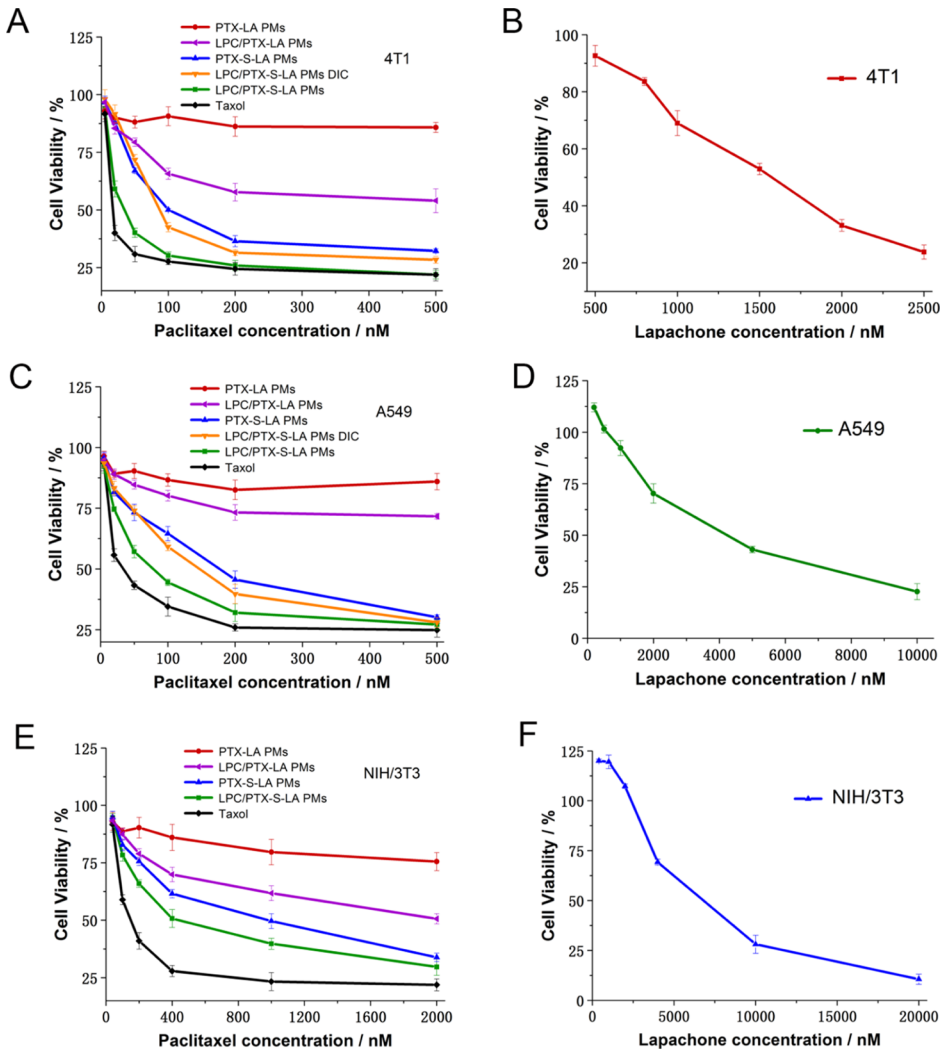

Figure 3. Cell viability of PTX-LA PMs, LPC/PTX-LA PMs, PTX-S-LA PMs, Taxol, and LPC/PTX-S-LA PMs with or without dicoumarol (DIC, a competitive inhibitor of NQO1) against 4T1 (A), A549 (C), and NIH 3T3 cells (E) at different concentrations after 48 h incubation. In vitro cytotoxicity of LPC against 4T1 (B), A549 (D), and NIH 3T3 cells (F) for 48 h.

Therefore, PEG−PDLLA micelles had much stronger cell uptake than C-6 solution.

Encouraged by cell uptake results, the PTX release amount was determined when incubated with 4T1, A549, and NIH

DOI: 10.1021/acsami.9b03056
ACS Appl. Mater. Interfaces XXXX, XXX, XXX−XXX

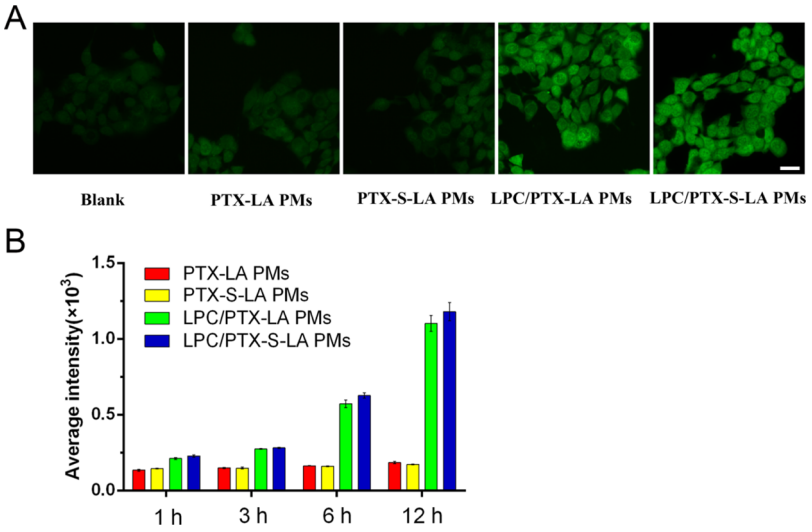

Figure 4. (A) Fluorescence microscopy images of 4T1 cancer cells staining with DCFH-DA after administration with PTX-LA PMs, PTX-S-LA PMs, LPC/PTX-LA PMs, and LPC/PTX-S-LA PMs for 3 h. Scale bar, 20 μm. (B) Cellular ROS generation of 4T1 cancer cells administrated with formulations for 1, 3, 6, and 12 h.

3T3 cells for 6 and 24 h. As shown in Figure 2D,E, PTX release from PTX-S-LA PMs was 10-fold greater than PTX-LA PMs and LPC/PTX-LA PMs at 6 and 24 h after incubation with 4T1 cells, respectively. Meanwhile, LPC/PTX-S-LA PMs released more PTX than PTX-S-LA PMs after 6 or 24 h incubation with 4T1 and A549 cells, agreeing well with in vitro release. Moreover, a remarkable faster PTX release rate of LPC/PTX-S-LA PMs was monitored in 4T1 and A549 cells than in NIH 3T3 cells, demonstrating that LPC/PTX-S-LA PMs exhibited distinct advantages in rapid PTX bioactivation in NQO1-overexpressed cancer cells.

3.6. Cytotoxicity Assays. The cytotoxicity was studied with 4T1, A549, and NIH 3T3 cells using MTT assay. The molar ratio of the PTX prodrug to LPC in the PMs was 1:3. IC_{50} of PTX-S-LA PMs against 4T1 cells and A549 cells was 126.7 and 176.2 nM at 48 h, respectively, exhibiting lower in vitro cytotoxicity in comparison with Taxol due to the delayed PTX release (Figure 3 and Table S1). Meanwhile, the LPC/PTX-S-LA PMs showed similar cancer cell killing ability compared with Taxol. By contrast, the IC_{50} of LPC/PTX-S-LA PMs in NIH 3T3 cells was analogous to that of PTX-S-LA PMs, demonstrating an obvious advantage of the safety for normal cells. Owing to the extremely slow release of PTX, PTX-LA PMs displayed negligible cell toxicity. Moreover, dicoumarol (DIC, a competitive inhibitor of NQO1, 70 μM) was co-added to prove the NQO1-bioactivated cytotoxicity of LPC/PTX-S-LA PMs. The cytotoxicity of LPC/PTX-S-LA PMs against cancer cells was declined remarkably in the presence of DIC.

To elucidate the synergy effects between LPC and PTX-S-LA, we calculated the combination index (CI) with the Chou–Talalay method, which is utilized to distinguish synergism, antagonism, and additivity between two used drugs. LPC/PTX-S-LA PMs had CI values of 0.39, 0.53, and 0.87 at 48 h against 4T1, A549, and NIH 3T3 cells, demonstrating good synergism as well as ultraselective cytotoxicity against cancer cells.

3.7. Intracellular ROS Production and NQO1 Level Quantification. NQO1-responsive ROS generation was detected with 4T1 cells and NIH 3T3 cells by 2,7-dichlorodihy-drofluorescein diacetate (DCFH-DA). The cells incubated in different formulations were detected with an inverted fluorescence microscope after DCFH-DA staining. The PTX-LA PMs and PTX-S-LA PMs did not enhance the intracellular ROS level, while LPC-loading PMs (LPC/PTX-LA PMs and LPC/PTX-S-LA PMs) significantly increased the green signal of DCF in 4T1 cells (Figures 4A and S6), demonstrating a higher intracellular ROS level elicited by loaded ROS-trigger LCP. Moreover, the intracellular ROS level was further quantified using flow cytometry at 1, 3, 6, and 12 h after treatment. The LPC-loading PMs considerably increased the ROS level compared with PTX-prodrug PMs in 12 h (Figure 4B), and the ROS fluorescence signal showed time-dependent increase for the LPC-loading PMs. By contrast, the fluorescence signal of NIH 3T3 cells after incubation with LPC/PTX-S-LA PMs showed negligible increase (Figure S5). Therefore, the LPC/PTX-S-LA PMs could effectively and selectively improve the ROS level of 4T1 cancer cells, which is helpful to bioactivate the ROS-responsive PTX-S-LA prodrug. We further quantified NQO1 levels using the ELISA kit. As shown in Figure S7, the NQO1 level of 4T1 and A549 was 25 and 19 times greater than that of NIH 3T3, respectively, leading to efficient and tumor-specific ROS production after administration with LPC-loading PMs.

3.8. Pharmacokinetics. The pharmacokinetic profiles of Taxol, LPC/PTX-S-LA PMs, and LPC/PTX-LA PMs were evaluated in rats. PTX eliminated readily after Taxol administration, exhibiting a short circulation time. In contrast, LPC/PTX-S-LA PMs and LPC/PTX-LA PMs showed prolonged retention in blood, with little PTX leaked from the PTX prodrug-loading PMs (Figure 5). As shown in Table S2, AUC of LPC/PTX-S-LA PMs and LPC/PTX-LA PMs was 11 times and 31.3 times higher than Taxol.

3.9. Biodistribution and PTX Release and LPC Accumulation in the Tumor. To investigate biodistribution, free DiR solution and DiR-labeled PEG–PDLLA micelles were administrated intravenously when the tumor volume of 4T1 bearing BALB/c mice reached about 300 mm^3. The fluorescent signals in tumors of DiR-labeled PEG–PDLLA PMs increased over time from 4 to 12 h (Figure 6A). As shown in Figure

DOI: 10.1021/acsami.9b03056
ACS Appl. Mater. Interfaces XXXX, XXX, XXX–XXX

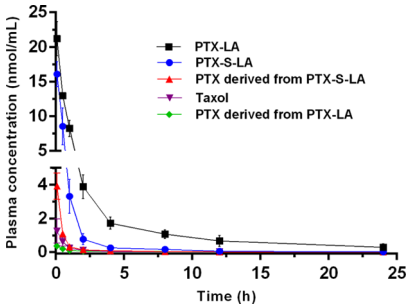

Figure 5. In vivo plasma concentration−time profiles of PTX and PTX prodrug when administrated with different formulations.

6B,C, DiR-labeled PEG−PDLLA micelles showed significantly higher fluorescent intensity in tumors at 24 h. In contrast, slight fluorescence was observed in the tumor at 24 h for free DiR solution. These data indicated that extended blood circulation time of PEG−PDLLA micelles ensured higher tumor accumulation mediated by the EPR effect, in agreement with the in vivo pharmacokinetic results.[23]

We further monitored the concentrations of released free PTX and LPC in the tumor. LPC/PTX-LA PMs and LPC/PTX-S-LA PMs displayed excellent tumor accumulation of LPC (Figure 6E). Moreover, PTX-LA PMs and LPC/PTX-LA PMs showed poor bioactivation in the tumor (Figure 6D). The released free PTX concentration of LPC/PTX-S-LA PMs was 2 times higher than that of PTX-S-LA PMs, indicating that LPC/PTX-S-LA PMs could accumulate in the tumor and bioactivate oxidation-responsive PTX-S-LA prodrug via NQO1-induced ROS production.

3.10. In Vivo Antitumor Studies. In vivo antitumor activity was studied with 4T1 tumor-bearing BALB/c female mice. PTX-LA PMs displayed a weak antitumor effect similar

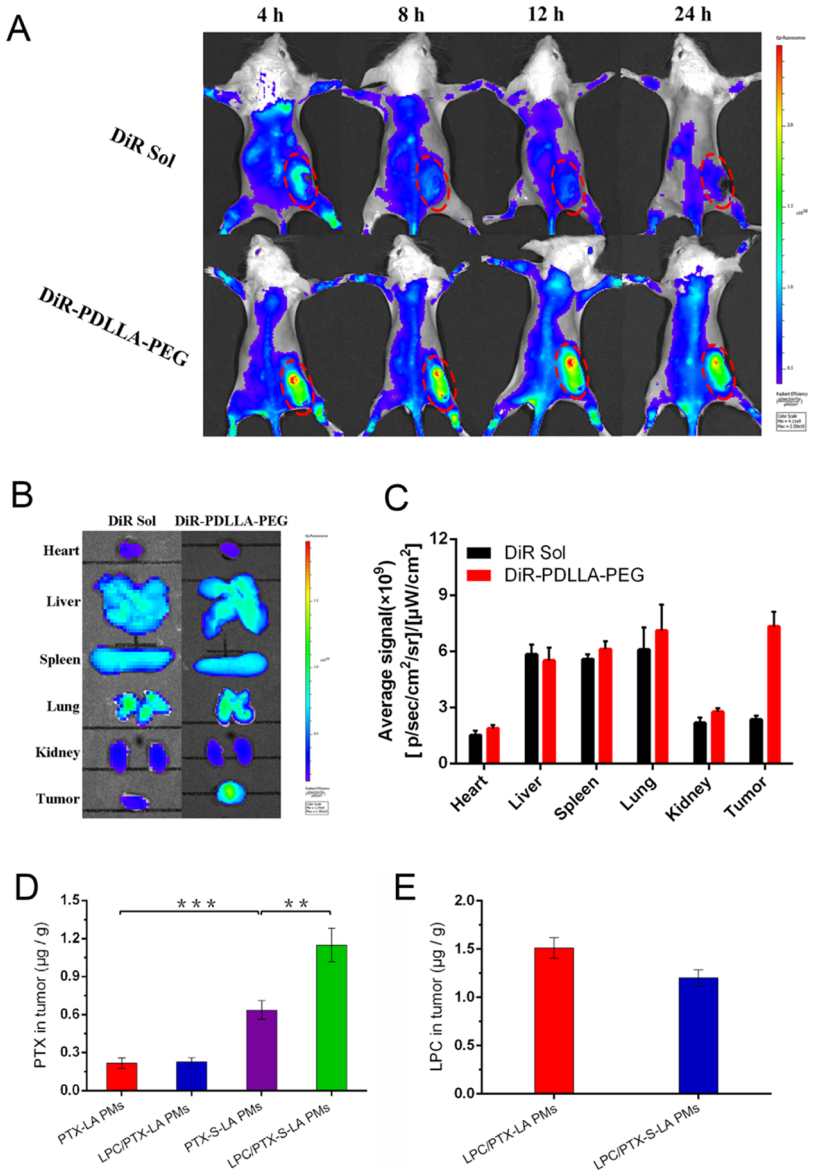

Figure 6. (A) Optical imaging of DiR solution and DiR-PDLLA−PEG PMs (2 mg kg^{-1} of DiR) for 4, 8, 12, and 24 h. The optical pictures were obtained at an excitation of 748 nm. Fluorescent imaging (B) and quantitative analysis (C) for biodistribution of DiR solution and DiR-PDLLA−PEG PMs (2 mg kg^{-1} of DiR) in 4T1-bearing BALB/c mice at 24 h (n = 3). Quantification of released free PTX (D) and LPC (E) in tumors at 12 h after administration. (***P < 0.001, **P < 0.01, n = 3).

DOI: 10.1021/acsami.9b03056
ACS Appl. Mater. Interfaces XXXX, XXX, XXX−XXX

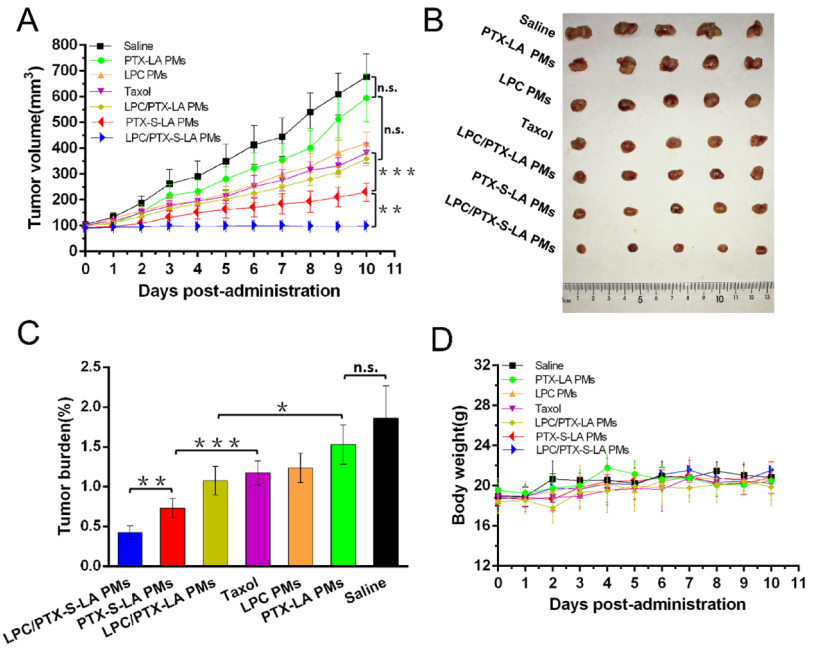

Figure 7. Anticancer efficacy of saline, PTX-LA PMs, LPC PMs, Taxol, LPC/PTX-LA PMs, PTX-S-LA PMs, and LPC/PTX-S-LA PMs administrated intravenously every other day against 4T1 cancer. (A) Tumor growth profiles treated with different formulations, (B) pictures of excised tumors, (C) tumor burden treated with different formulations, (D) body weight changes during treatments.

to saline, demonstrating that the ester bond linked non-sensitive PTX-LA prodrug was too stable to release PTX efficiently in vivo. Besides, LPC PMs, Taxol, and LPC/PTX-LA PMs showed a similar moderate anticancer effect with delayed tumor growth. Moreover, PTX-S-LA PMs showed the greater antitumor effect than Taxol and LPC/PTX-LA PMs in the suppression of tumor growth, which was ascribed to the high tumor accumulation and on-site bioactivation of PTX-S-LA by the endogenous relative high ROS level in tumor cells.[24] Notably, LPC/PTX-S-LA PMs showed the best antitumor effect among all the studied formulations because of rapid on-site PTX-S-LA bioactivation triggered by the further elevated ROS level mediated by LPC, agreeing well with the in vitro cytotoxicity and release results.

The safety of LPC/prodrug PMs was evaluated through monitoring body weight and H&E stained tissue slices. No remarkable body weight variation was found for the studied formulations (Figure 7D). Besides, Figure S8 displayed no noticeable abnormality of H&E stained slices for vital organs, while H&E stained tumor slices indicated that the LPC/PTX-S-LA PMs group showed obviously decreased cellularity, serious vacuolization, and shrinking nucleus, demonstrating severe and widespread apoptosis of the cancer cells.

4. CONCLUSIONS

Herein, we integrated NQO1-responsive ROS production and ROS-triggered prodrug chemotherapy into the self-strengthened bioactivating prodrug nanosystem to realize high anticancer efficacy. The prodrug nanosystem exhibited a sequential release behavior, which release LPC first to trigger the synergistically facilitated release of ROS-activated PTX-S-LA by catalysis of NQO1. Given much higher cellular uptake efficiency, self-strengthened prodrug bioactivation, ultraselective release and cytotoxicity between cancer and normal cells, obvious intracellular ROS production in 4T1 cancer cells, prolonged systemic circulation, and enhanced tumor accumulation, LCP/PTX-S-LA PMs demonstrated the best in vivo anticancer efficacy in 4T1 xenograft mice. Thus, the self-strengthened bioactivating prodrug nanosystem provides new ideas for rational design of oxidation-responsive prodrug-based NPs with enhanced anticancer activity and low toxicity.

■ ASSOCIATED CONTENT

Supporting Information

The Supporting Information is available free of charge on the ACS Publications website at DOI: 10.1021/acsami.9b03056.

Synthetic routes, mass spectrum, and NMR spectrum of PTX-LA and PTX-S-LA; colloidal stability of LPC/prodrug PMs; mean fluorescence intensity of microscopy images; fluorescence microscopy images and flow cytometric analysis for intracellular ROS of NIH 3T3 cells; NQO1 levels quantification; H&E staining of the major organs and tumors; cytotoxicity of Taxol, LPC, and prodrug micelles; pharmacokinetic parameters of Taxol and LPC/prodrug PMs (PDF)

■ AUTHOR INFORMATION

Corresponding Authors

*E-mail: wangduncn@hotmail.com. Phone: +86-024-23986428. Fax: +86-024-23986428 (D.W.).
*E-mail: sunjin@syphu.edu.cn. Phone: +86-024-23986321. Fax: +86-024-23986321 (J.S.).

ORCID

Jin Sun: 0000-0001-5470-1599

Author Contributions

¶K.W. and B.Y. contributed equally to this work.

Notes

The authors declare no competing financial interest.

DOI: 10.1021/acsami.9b03056
ACS Appl. Mater. Interfaces XXXX, XXX, XXX−XXX

■ ACKNOWLEDGMENTS

This work was supported by National Natural Science Foundation of China (nos. 81872816, 81773656, 81703451).

■ REFERENCES

(1) Chen, Q.; Liu, G.; Liu, S.; Su, H.; Wang, Y.; Li, J.; Luo, C. Remodeling the Tumor Microenvironment with Emerging Nanotherapeutics. *Trends Pharmacol. Sci.* **2018**, *39*, 59−74.

(2) Luo, C.; Sun, J.; Sun, B.; Liu, D.; Miao, L.; Goodwin, T. J.; Huang, L.; He, Z. Facile Fabrication of Tumor Redox-Sensitive Nanoassemblies of Small-Molecule Oleate Prodrug as Potent Chemotherapeutic Nanomedicine. *Small* **2016**, *12*, 6353−6362.

(3) Sun, B.; Luo, C.; Yu, H.; Zhang, X.; Chen, Q.; Yang, W.; Wang, M.; Kan, Q.; Zhang, H.; Wang, Y.; He, Z.; Sun, J. Disulfide Bond-Driven Oxidation- and Reduction-Responsive Prodrug Nanoassemblies for Cancer Therapy. *Nano Lett.* **2018**, *18*, 3643−3650.

(4) Wei, W.; Luo, C.; Yang, J.; Sun, B.; Zhao, D.; Liu, Y.; Wang, Y.; Yang, W.; Kan, Q.; Sun, J.; He, Z. Precisely Albumin-Hitchhiking Tumor Cell-Activated Reduction/Oxidation-Responsive Docetaxel Prodrugs for the Hyperselective Treatment of Breast Cancer. *J. Controlled Release* **2018**, *285*, 187−199.

(5) Han, H.; Wang, H.; Chen, Y.; Li, Z.; Wang, Y.; Jin, Q.; Ji, J. Theranostic Reduction-Sensitive Gemcitabine Prodrug Micelles for Near-Infrared Imaging and Pancreatic Cancer Therapy. *Nanoscale* **2016**, *8*, 283−291.

(6) Zhang, D.; Yang, J.; Guan, J.; Yang, B.; Zhang, S.; Sun, M.; Yang, R.; Zhang, T.; Zhang, R.; Kan, Q.; Zhang, H.; He, Z.; Shang, L.; Sun, J. In vivo tailor-made protein corona of a prodrug-based nanoassembly fabricated by redox dual-sensitive paclitaxel prodrug for the superselective treatment of breast cancer. *Biomater. Sci.* **2018**, *6*, 2360−2374.

(7) Li, M.; Zhao, L.; Zhang, T.; Shu, Y.; He, Z.; Ma, Y.; Liu, D.; Wang, Y. Redox-Sensitive Prodrug Nanoassemblies Based on Linoleic Acid-Modified Docetaxel to Resist Breast Cancers. *Acta Pharm. Sin. B* **2019**, *9*, 421−432.

(8) Li, J.; Sun, C.; Tao, W.; Cao, Z.; Qian, H.; Yang, X.; Wang, J. Photoinduced PEG Deshielding from ROS-Sensitive Linkage-Bridged Block Copolymer-Based Nanocarriers for On-Demand Drug Delivery. *Biomaterials* **2018**, *170*, 147−155.

(9) Kim, J.; Lee, J.; Lee, Y. M.; Pramanick, S.; Im, S.; Kim, W. J. Andrographolide-Loaded Polymerized Phenylboronic Acid Nanoconstruct for Stimuli-Responsive Chemotherapy. *J. Controlled Release* **2017**, *259*, 203−211.

(10) Pei, Y.; Li, M.; Hou, Y.; Hu, Y.; Chu, G.; Dai, L.; Li, K.; Xing, Y.; Tao, B.; Yu, Y.; Xue, C.; He, Y.; Luo, Z.; Cai, K. An Autonomous Tumor-Targeted Nanoprodrug for Reactive Oxygen Species-Activatable Dual-Cytochrome C/Doxorubicin Antitumor Therapy. *Nanoscale* **2018**, *10*, 11418−11429.

(11) Yang, B.; Wang, K.; Zhang, D.; Sun, B.; Ji, B.; Wei, L.; Li, Z.; Wang, M.; Zhang, X.; Zhang, H.; Kan, Q.; Luo, C.; Wang, Y.; He, Z.; Sun, J. Light-Activatable Dual-Source ROS-Responsive Prodrug Nanoplatform for Synergistic Chemo-Photodynamic Therapy. *Biomater. Sci.* **2018**, *6*, 2965−2975.

(12) Ma, X.; Moore, Z. R.; Huang, G.; Huang, X.; Boothman, D. A.; Gao, J. Nanotechnology-Enabled Delivery of NQO1 Bioactivatable Drugs. *J. Drug Targeting* **2015**, *23*, 672−680.

(13) Zhang, K.; Chen, D.; Ma, K.; Wu, X.; Hao, H.; Jiang, S. NAD(P)H:Quinone Oxidoreductase 1 (NQO1) as a Therapeutic and Diagnostic Target in Cancer. *J. Med. Chem.* **2018**, *61*, 6983−7003.

(14) Blanco, E.; Bey, E. A.; Dong, Y.; Weinberg, B. D.; Sutton, D. M.; Boothman, D. A.; Gao, J. β-Lapachone-containing PEG-PLA polymer micelles as novel nanotherapeutics against NQO1-overexpressing tumor cells. *J. Controlled Release* **2007**, *122*, 365−374.

(15) Blanco, E.; Bey, E. A.; Khemtong, C.; Yang, S. G.; Setti-Guthi, J.; Chen, H.; Kessinger, C. W.; Carnevale, K. A.; Bornmann, W. G.; Boothman, D. A.; Gao, J. β-Lapachone Micellar Nanotherapeutics for Non-Small Cell Lung Cancer Therapy. *Cancer Res.* **2010**, *70*, 3896−3904.

(16) Gaucher, G.; Marchessault, R. H.; Leroux, J.-C. Polyester-Based Micelles and Nanoparticles for the Parenteral Delivery of Taxanes. *J. Controlled Release* **2010**, *143*, 2−12.

(17) Ye, M.; Han, Y.; Tang, J.; Piao, Y.; Liu, X.; Zhou, Z.; Gao, J.; Rao, J.; Shen, Y. A Tumor-Specific Cascade Amplification Drug Release Nanoparticle for Overcoming Multidrug Resistance in Cancers. *Adv. Mater.* **2017**, *29*, 1702342.

(18) Luo, C.; Sun, J.; Liu, D.; Sun, B.; Miao, L.; Musetti, S.; Li, J.; Han, X.; Du, Y.; Li, L.; Huang, L.; He, Z. Self-Assembled Redox Dual-Responsive Prodrug-Nanosystem Formed by Single Thioether-Bridged Paclitaxel-Fatty Acid Conjugate for Cancer Chemotherapy. *Nano Lett.* **2016**, *16*, 5401−5408.

(19) Zhang, X.; Sun, B.; Zuo, S.; Chen, Q.; Gao, Y.; Zhao, H.; Sun, M.; Chen, P.; Yu, H.; Zhang, W.; Wang, K.; Zhang, R.; Kan, Q.; Zhang, H.; He, Z.; Luo, C.; Sun, J. Self-Assembly of a Pure Photosensitizer as a Versatile Theragnostic Nanoplatform for Imaging-Guided Antitumor Photothermal Therapy. *ACS Appl. Mater. Interfaces* **2018**, *10*, 30155−30162.

(20) Zhang, L.; Chen, Z.; Yang, K.; Liu, C.; Gao, J.; Qian, F. β-Lapachone and Paclitaxel Combination Micelles with Improved Drug Encapsulation and Therapeutic Synergy as Novel Nanotherapeutics for NQO1-Targeted Cancer Therapy. *Mol. Pharm.* **2015**, *12*, 3999−4010.

(21) Zhang, L.; Sun, H.; Chen, Z.; Liu, Z.; Huang, N.; Qian, F. Intermolecular Interactions between Coencapsulated Drugs Inhibit Drug Crystallization and Enhance Colloidal Stability of Polymeric Micelles. *Mol. Pharm.* **2017**, *14*, 3568−3576.

(22) Zhang, S.; Guan, J.; Sun, M.; Zhang, D.; Zhang, H.; Sun, B.; Guo, W.; Lin, B.; Wang, Y.; He, Z.; Luo, C.; Sun, J. Self-Delivering Prodrug-Nanoassemblies Fabricated by Disulfide Bond Bridged Oleate Prodrug of Docetaxel for Breast Cancer Therapy. *Drug Delivery* **2017**, *24*, 1460−1469.

(23) Sun, Q.; Zhou, Z.; Qiu, N.; Shen, Y. Rational Design of Cancer Nanomedicine: Nanoproperty Integration and Synchronization. *Adv. Mater.* **2017**, *29*, 1606628.

(24) Ramasamy, T.; Ruttala, H. B.; Gupta, B.; Poudel, B. K.; Choi, H.-G.; Yong, C. S.; Kim, J. O. Smart Chemistry-Based Nanosized Drug Delivery Systems for Systemic Applications: A Comprehensive Review. *J. Controlled Release* **2017**, *258*, 226−253.

DOI: 10.1021/acsami.9b03056
ACS Appl. Mater. Interfaces XXXX, XXX, XXX−XXX